Published version: doi.org/10.1016/j.elstat.2014.06.011

Continuous droplets' charge method for the Lagrangian simulation of electrostatic sprays

Jordi Grifoll[a] and Joan Rosell-Llompart[a,b] *

[a]DEW Laboratory, Chemical Engineering Department, Universitat Rovira i Virgili, 43007 Tarragona, Catalunya, Spain

[b]Catalan Institution for Research and Advanced Studies (ICREA), 08010 Barcelona, Catalunya, Spain

e-mail addresses: jordi.grifoll@urv.cat , joan.rosell@urv.cat
* corresponding author. Tel. +34-977-558-660; fax: +34-977-559-621

Keywords: electrospray; Poisson's equation; spray dynamics; numerical simulation; Lagrangian simulation

Abstract

A main drawback of classical simulation of electrostatic sprays based on the Lagrangian description of droplet trajectories is the large number of droplet-to-droplet electrical interactions that must be computed. We present and assess a new methodology in which some of these interactions are computed using a mean electrical field due to the droplets space charge considered as a continuum. This method has been applied to two systems, comprising 26000 droplets and 3500 droplets, resulting in 112 and 9 times faster computation, without loosing accuracy, as demonstrated in the predictions of impinging flux, droplet number density, and local droplet diameter. **1. Introduction**

Electrostatic spraying of liquids from electrified capillary tubes can result in quasi-monodispersed droplets with diameters ranging from nanometers to micrometers (Jaworek, 2008). The electrical charge carried by the droplets prevents their coalescence, and enables the control of the droplets' trajectories by means of electrodes.

These properties are critical in the technique of electrospray ionization mass spectrometry (ESI-MS) (Fenn, 2003), in the electrospray production of pharmaceutical particles (Peltonen *et al.*, 2010; Enayati *et al*., 2011; Bock *et al.*, 2012; Zamani *et al.*, 2013), and other electrospray applications such as micro- or nanoparticles and thin coatings (Barrero and Loscertales, 2007; Jaworek, 2007 a, b; Rietveld *et al.*, 2009; Martin *et al*., 2010; Bodnár and Rosell-Llompart, 2013).

The numerical simulation of electrospray systems, which are characterized by a large number of design variables, helps to reduce the number of experimental tests needed when developing designs for specific applications. In addition, numerically simulated systems can be interrogated in much more detail than experimental systems.

The most detailed mathematical descriptions available for simulating droplets plume dynamics are based on Lagrangian models, which track the forces acting on each droplet, and predict the resulting individualized droplets' motions (Gañán-Calvo et al., 1994; Hartman *et al.*, 1999; Wilhem *et al.*, 2003; Grifoll and Rosell-Llompart, 2012). Such individualized tracking of the droplets is straightforward to model; however, the numerical simulation of practical systems is hampered by long computation times (CPU times).

At the root of this problem is the requirement to compute $N(N-1)/2$ droplet-droplet electrostatic interactions at each time step of the computation, for N droplets in the plume. For instance, as reported by Grifoll and Rosell-Llompart (2012), a simulation of 0.2 seconds of an electrospray comprising 26000 droplets took 1658 hours of CPU time for an integration time step of 1 μs. This 0.2 s period covered the transient and a portion of the steady state needed to generate a statistically significant sample of independent snapshots of the charged spray.

The challenge of describing electrospray plumes with reasonable CPU times has motivated several studies. Higuera (2012, 2013) has proposed an Eulerian (continuum) model for a dilute spray, which gives realistic results at a fraction of the computational cost of a Lagrangian simulation. The Eulerian model can be applied in the regions where the fluctuations of the droplet velocity are negligible over its local average; for example, away from the droplet formation region.

Within the Lagrangian framework, Yang *et al.* (2012) have used graphics processing units (GPUs) to simulate millions of droplets trajectories with a (theoretical) computational power of 10 Tera FLOPS. Currently, this promising alternative to CPU-based calculations must be coded using a low-level assembly language that runs on both GPUs and CPUs.

Another Lagrangian methodology, implemented by Grifoll and Rosell-Llompart (2012) on a standard computer (single CPU), is based on a coarse-grained description of the electrical forces due to faraway droplets. This approach reduced the CPU time by a factor of 40 for the aforementioned example of 26000 droplets. Yet, these gains in CPU time could still be insufficient for practical scenarios, in which droplets can easily number in the hundreds of thousands in a single electrospray.

The present study aims to further reduce the CPU time in the Lagrangian framework, by implementing a continuous description of the electrical field created by the droplets' charge (*space charge*). In previous studies, and for computational purposes, the *total electrical field* sensed by each droplet is split into an *external field*, generated by the static parts of the system (electrodes), and a *space charge field* due to the droplets charge. In our proposal the *total electrical field* is computed from a continuous charge distribution which represents the droplets' charge, and is updated periodically.

2 Model and Governing Equations

2.1 Lagrangian Model

Electrostatically charged droplets are injected into the system near the end of an electrified capillary tube, which holds a conical liquid meniscus called a Taylor cone (Fernández de la Mora, 2007). The droplets travel towards a collection plate which is Earth-grounded. The Lagrangian model describes the droplets' spray plume as a *N*-body system governed by Newton's laws of motion

$$\frac{d\mathbf{R}_i}{dt} = \mathbf{V}_i \tag{1a}$$

$$m_i \frac{d\mathbf{V}_i}{dt} = \mathbf{F}_i \tag{1b}$$

where $\mathbf{R}_i = (x_i, y_i, z_i)$ is the position vector of droplet i (m), m_i is its mass (kg), $\mathbf{V}_i$ its velocity (m/s), and $\mathbf{F}_i$ is the sum of all forces acting on it (N). In this study, the *z* axis coincides with the capillary tube axis, and *x* and *y* are transversal axes. The resultant force can be decomposed as

$$\mathbf{F}_i = \mathbf{F}_{\mathbf{D}i} + \mathbf{F}_{\mathbf{elec}i} \tag{2}$$

where $\mathbf{F}_{\mathbf{D}i}$ is the drag force arising from the droplet's motion relative to its gas surroundings (N), and $\mathbf{F}_{\mathbf{elec}i}$ is the electrical force (N) experienced by droplet *i*. Considering the droplets as spherical particles surrounded by a still gas, the drag force is calculated as

$$\mathbf{F}_{\mathbf{D}i} = -C_{Di} \frac{\pi}{8} d_i^2 \rho_g \mathbf{V}_i |\mathbf{V}_i| \tag{3}$$

where the drag coefficient, C_{Di}, has been estimated from (Abraham, 1970)

$$C_{Di} = \frac{24}{Re_i}\left(1 + 0.1104\sqrt{Re_i}\right)^2 \tag{4}$$

valid for Reynolds number $Re_i = |\mathbf{V}_i| d_i \rho_g / \mu_g < 5000$. In the above equations, d_i denotes the particle diameter (m), μ_g (Pa·s) is the dynamic viscosity of the gas and ρ_g is the gas density (kg/m^3). While the restriction of still gas can be relaxed as shown by Arumugham-Achari *et al.* (2013), in the present work we have kept it for simplicity.

The electrical force experienced by droplet *i* is the product of the droplet charge q_i times the electrical field at the droplet's position $\mathbf{E}(\mathbf{R}_i)$:

$$\mathbf{F}_{\mathbf{elec}\,i} = q_i \cdot \mathbf{E}(\mathbf{R}_i) \tag{5}$$

Depending on how the electrical field is calculated, one can distinguish different submodels, as described next.

2.2 Discrete Charge Submodel

This is the classical approach adopted in most previous Lagrangian simulations of electrosprays. The electrical field sensed by a droplet *i*, $\mathbf{E}(\mathbf{R}_i)$ in equation (5), is computed as the sum of the so-called *external* electrical field at the droplet's position ($\mathbf{E}_{\mathbf{ext}}(\mathbf{R}_i)$) due to the static structure (usually, electrodes), plus the field created by the *space charge* associated with all the other droplets in the spray plume and their images on the collection plate:

$$\mathbf{E}(\mathbf{R}_i) = \mathbf{E}_{\mathbf{ext}}(\mathbf{R}_i) + \mathbf{E}_{\mathbf{sc}i} \tag{6}$$

$\mathbf{E}_{\mathbf{ext}}(\mathbf{R}_i)$ is minus the gradient of the electrical potential which is found by solving Laplace's equation (excluding the spray charges), with appropriate conditions at the static boundaries. $\mathbf{E}_{\mathbf{sc}i}$, on the other hand, is calculated by adding all of the contributions from the other droplet charges (Grifoll and Rosell-Llompart, 2012):

$$\mathbf{E}_{\mathbf{sc}i} = \frac{1}{4\pi\varepsilon}\left[\sum_{i\neq j}^{N} q_j\left(\frac{\mathbf{R}_{ij}}{R_{ij}^3} - \frac{\mathbf{R}_{iJ}}{R_{iJ}^3}\right) - q_i\frac{\mathbf{R}_{iI}}{R_{iI}^3}\right] \tag{7}$$

where $\mathbf{R}_{ij} = \mathbf{R}_i - \mathbf{R}_j$ is the displacement vector between the position vectors of droplets *j* and *i* (m), $\mathbf{R}_{iJ} = \mathbf{R}_i - \mathbf{R}_J$ is the displacement vector between the position vectors of the image of droplet *j*, which is positioned inside the collection plate at $\mathbf{R}_J = \left(x_j, y_j, 2H - z_j\right)$, and droplet *i* (m) (where H is the separation between the capillary end and the collection plate), ε is the gas permittivity (taken for air as 8.854×10^{-12} A s/V m) and N is the total number of droplets in the plume. As mentioned in the Introduction, it is the computation of the $\mathbf{E}_{\mathbf{sc}i}$ term through equation (7) that significantly slows down the overall computation.

Figure 1(a) shows the modulus of the transversal component of the space charge field $E_{sct} = \sqrt{E_{scx}^2 + E_{scy}^2}$ experienced by three droplets as they travel through a spray previously simulated by Grifoll and Rosell-Llompart (2012) using the Discrete Charge submodel (therein used in the so called "complete simulation"). The trajectories of the droplets projected on the (*r*, *z*)-plane are shown in Figure 1(b) overlaid with a snapshot of the spray plume.

The transversal field modulus E_{sct} is smooth far away from the centerline, but it is jagged close to the centerline, due to the influence of neighboring droplets. Similar trends have been found in analyses of other droplets' trajectories, not shown. The finding that the electrical field is very smooth within a large portion of the spray (away from the centerline) suggests that a continuous description of the electrical field can be adopted in this region. This possibility is explored in the next subsection.

2.3 Continuous Charge submodel

A local continuous density of charge, ρ (C/m^3), and the electrical potential ϕ (V) satisfy Poisson's equation:

$$\nabla^2\phi = -\frac{\rho}{\varepsilon} \tag{8}$$

from whose solution the electrical field can be calculated with

$$\mathbf{E} = -\nabla\phi \tag{9}$$

However, upon injection, the droplets are organized nearly in a line (Tang and Gomez, 1994); therefore, the space charge density is ill defined there. Moreover, as seen in Figure 1, the electrical field for droplets close to the centerline fluctuates strongly. These fluctuations are due to interactions with neighboring droplets, and it is clear that they would not be properly described by a simple continuous description.

Therefore, our proposal computes the electrical field experienced by a droplet differently depending on its location, which is either near the centerline (within an inner region RI defined by radius $r \le r^*$) or away from it (within an outer region RO defined by radius $r > r^*$). Droplets within RO sense a continuous electrical field generated by a continuous charge distribution which is a function of position, mimicking the discrete charge carried by the droplets. Therefore, this field is the solution to equations (8-9) using appropriate boundary conditions at the electrodes. On the other hand, droplets within RI sense both a *continuous* electrical field due to a continuous charge density associated to droplets in RO, and a *grainy* electrical field due to individual droplets in RI. Mathematically,

$$\mathbf{E}(\mathbf{R}_i) = \mathbf{E}_{\mathbf{RO}}(\mathbf{R}_i) + \mathbf{E}_{\mathbf{RI}i} \tag{10}$$

where,

$$\nabla^2 \phi_{RO} = -\frac{\rho_{RO}}{\varepsilon} \tag{11}$$

$$\mathbf{E_{RO}} = -\nabla \phi_{RO} \tag{12}$$

and

$$\mathbf{E_{RI}}_i = \frac{1}{4\pi\varepsilon}\left[\sum_{i\neq j}^{N_{RI}} q_j \left(\frac{\mathbf{R}_{ij}}{R_{ij}^3} - \frac{\mathbf{R}_{iJ}}{R_{iJ}^3}\right) - q_i \frac{\mathbf{R}_{iI}}{R_{iI}^3}\right] \tag{13}$$

where ρ_{RO} is the continuous charge density associated *only* to droplets in RO (namely, with ρ_{RO} taken to be equal to zero in region RI). In Eq. (13) the summation is extended only to the N_{RI} droplets which exist within region RI.

It should be noted that when solving equation (8), the image charge induced on the electrodes (spraying capillary tube included) is automatically accounted for, while the Discrete Charge submodel neglects the image charge on the capillary tube. When solving Eq. (11) the image charge induced on the capillary tube by droplets in region RO is also accounted for.

2.4 Numerical Implementation

The Discrete Charge submodel (#2.2) has been implemented as in our earlier work (Grifoll and Rosell-Llompart, 2012). Equations (1)-(5) are solved starting with a droplet-free domain at time $t = 0$. Droplets are injected near the Taylor cone tip according to the injection rules presented in that article.

The key advantage of the Continuous Charge submodel (#2.3) is the fact that it is not necessary to solve equations (8) and (11) at every integration time step. Global changes in the electrical field can only occur through restructuring of the spray, which can develop over time scales that are much longer than the integration time step. Therefore,

these equations are solved every M time steps, so that the electrical field is updated with a frequency high enough to capture the electrical field dynamics, which is of order the inverse of the lifetime of a typical droplet (travel time from injection to collection). Since this lifetime is much longer than the integration time step, the former being of the order of milliseconds and the latter of microseconds, M can be of the order of thousands. As will be shown, such large values of M result in significant CPU time savings.

Poisson's equation (Eqs. (8) & (11)) has been solved in non-homogeneous finite volume discretization, using axisymmetric cylindrical coordinates, with boundary conditions $\phi = \Phi_0$ at the wall of the cylindrical capillary tube (which is centered on the *z*-axis, and extends over $z < 0$) and Taylor cone external surfaces, $\phi = 0$ V at the collection plate ($z = H$), $\partial\phi/\partial z = 0$ at $z = -10H$, and $\partial\phi/\partial r = 0$ at $r = 10H$. Because the electrodes have cylindrical symmetry, we hypothesize that the continuous droplets charge density distributions, ρ and ρ_{RO}, also have cylindrical symmetry. Therefore, we have discarded the azimuthal component when solving Equations (8) and (11).

3. Results and discussion

We have compared the results from the Discrete Charge and the Continuous Charge submodels for two real electrospray systems, which are characterized by the parameters listed in Table 1 (Grifoll and Rosell-Llompart, 2012). In both cases, the simulations were run for electrospray time running between $t = 0$ and 0.6 s, and the steady state was found to start at approximately $t = 0.1$ s, according to the criterion given in Grifoll and Rosell-Llompart (2012). Except for CPU time data, which include the initial transient

($0 < t < 0.1$ s), all of the graphs and data discussed in this section refer to the steady state part of this period.

Table 1. Parameters characterizing the simulated spray systems

	Case 1	Case 2
Reference	Park *et al.*, (2004)	Tang and Gomez, (1994)
Liquid density (kg/m^3), ρ	789.4	685
Liquid flow rate (m^3/s), Q	0.333×10^{-9}	2.78×10^{-9}
Outer capillary tube diameter (m)	9×10^{-4}	4.5×10^{-4}
Capillary tube to collection plate distance (m), H	0.03	0.03
Capillary tube potential (V), Φ_0	4000[†]	5000[†]
Electric current intensity (A), I	37.4×10^{-9}	n.g.[¥]
Primary droplet count mean diameter (m)	8.84×10^{-6}	3.24×10^{-5}
Primary drop diameter RMS (%)	20.9	2.02
Satellite droplet count mean diameter (m)	n.a.[§]	9.93×10^{-6}
Satellite drop diameter RMS (%)	n.a.[§]	25%
Jet break up position (m), z_0	0.5×10^{-3}[#]	2.4×10^{-3}[£]
Jet velocity (m/s), v_0	19.4	12.0

[†]Referred to collection plate potential of 0 V.
[§]n.a.: not applicable.
[¥]n.g.: not given.
[#]This value is chosen *ad hoc* at $13.5\times \bar{d}$ plus the Taylor cone height (0.39 mm).
[£]Taken from Fig. 7 of Tang and Gomez (1994).

3.1 Case 1

Case 1 is based on one of the electrosprays described by Park *et al.* (2004). We have focused our method development on this case because this is the electrospray with the largest droplet population studied here.

3.1.1 Selection of the number of snapshots needed for charge density averaging

The charge density fields (ρ and ρ_{RO}) needed to solve equations (8) and (11) have been found using the last snapshot available. Under steady state, no significant difference has been found between solutions based on charge density fields based on a single snapshot or based on the averaging of many snapshots (~500). (Throughout the simulation, a snapshot of the spray, consisting of all the droplets' positions and velocities, is recorded every 2×10^{-4} spray-time seconds.) Figure 2(a) shows that using a single snapshot to build the charge density field, results in isopotential lines that are smooth. This solution (taken from the simulation using the Discrete Charge submodel) is indistinguishable from the solution based on averaging 500 snapshots (not shown).

That the space charge contributes significantly to this field can be seen by comparison of this panel with panel (b), which shows the isolines that are only associated to the external field (due to the electrodes).

3.1.2 Selection of regions RI and RO

For selecting regions RI and RO, it is helpful to investigate the fluctuating nature of the electrical field experienced by the droplets as a function of the radial coordinate. This calculation has been performed using snapshots from a Discrete Charge submodel simulation in order to properly capture the fluctuations arising from droplet-droplet interactions. Figure 3 shows the radial distribution of the average and the root mean square (RMS) of the modulus of the transversal electrical field, $E_t = \sqrt{E_x^2 + E_y^2}$, where E_x and E_y are the non-axial components of $\mathbf{E}(\mathbf{R}_i)$, computed using Eq. (6). In

this graph, we consider the droplets found within a slice z = 15 mm ± 0.5 mm in 2500 snapshots.

As the centerline is approached, the average modulus decreases while the RMS increases to comparable values or even higher. As discussed earlier in the context of Figure 1, such fluctuations in the electrical field are associated with local non-homogeneities of the droplets' space charge.

The boundary between regions RI and RO should separate the region RI, where the fluctuations are important, from the RO region, where $\overline{E}_t$ should be much greater than RMS(E_t). Therefore, Figure 3 suggests, for this spray, that such boundary should be at a radius *r** equal to a few mm. In this work we have used a standard value of *r** = 3 mm (where in Figure 3, $RMS(E_t)/\overline{E}_t = 15\%$).

3.1.3 Selection of integration time step and electrical field update time

According to Grifoll and Rosell-Llompart (2012) a convenient integration time step for this case is 1×10^{-6} s. This choice is dictated by the fast droplet dynamics close to the injection point. Therefore, we have adopted the same integration time step.

The effect of the electrical field update time has been studied, for *M* ranging between 2500 and 10000 (and *r** between 1 and 3 mm). Very similar results have been obtained in all of these simulations; therefore, we have selected *M* = 5000 as a standard value in this work.

3.1.4 Comparison of the two submodels

Figure 4 shows the radial distributions of the droplet volumetric flux impinging onto the collection plate, as predicted using the Discrete Charge submodel and the Continuous Charge submodel (for $r^* = 3$ and 1 mm; $M = 5000$). The uncertainty bars have been estimated according to the procedure outlined in appendix A.

Using $r^* = 3$ mm, the prediction agrees very well with the Discrete Charge submodel, although the CPU time taken by this simulation was only 0.9% that required when using the Discrete Charge submodel. The maximum discrepancy (from the Discrete Charge submodel) is only -3.6% at $r = 3.8$ mm. Using $r^* = 1$ mm, the prediction is still quite good (with maximum relative discrepancy of -5.8% at $r = 2.4$ mm). Relative to the Discrete Charge submodel prediction, both of these cases underestimate the flux close to $r = r^*$, while this deficit is compensated by a flux surplus at the spray periphery, resulting in a slightly expanded spray.

Further confirmation of equivalence between the two submodels is provide in Figures 5 and 6, which show contour plots of the predicted locally-averaged droplet number density and droplet diameter, respectively.

On the other hand, using $r^* = 0$ mm resulted in poorly predicted spray dynamics, characterized by depletion of droplets from the central region, non monotonous droplet number density, and oscillations in the number of droplets in the spray (data not shown).

We have also checked that using either $M = 2500$ or 10000 lead to very similar results, including predictions within the initial transient. In these two simulations (with $r^* = 3$ mm), the CPU times were 30% longer and 15% shorter, respectively, than the $M = 5000$ run (31 hours).

In sum, these results lead us to conclude that the method based on the Continuous Charge submodel is robust and accurate for the simulation of Case 1, while it needs only a small fraction of the CPU time taken by the classical approach.

3.2 Case 2

Figure 7 shows two snapshots of the Tang and Gomez (1994) electrospray in the steady state, which has been simulated both using the Discrete Charge submodel (Fig. 7(a)), and the Continuous Charge submodel (Fig. 7(b)). These snapshots are characterized by a central plume of primary droplets, surrounded by a shroud of satellite droplets, as found experimentally by Tang and Gomez (1994).

Figure 8 shows the predicted radial distribution of the corresponding volumetric impinging flux associated to the droplets impinging on the collection plate. Excellent agreement is found between the simulations based on the Discrete Charge and the Continuous Charge submodels, with maximum disagreement near the central region of 2.3%.

In view of these results, we conclude, also for Case 2, that the method based on the Continuous Charge submodel is robust and accurate.

3.3 Computational efficiency

Table 2 compares the times taken by the various simulations based on the Discrete Charge and Continuous Charge submodels. We can see that the computations based on the Continuous Charge submodel are much faster than those based on the Discrete Charge submodel. This improvement is the net result of having greatly reduced the number of droplet-pair interactions computed at each step, despite having to solve

Poisson's equation twice every *M* time steps. Such interactions are now computed only among droplets within region RI, which are a fraction of the total number of droplets (7.5% for Case 1, 10% for Case 2). It should also be noted that the standard values for the *r** and *M* parameters have not been optimized. Moreover, we have seen that there is room for optimization, since halving *r** and doubling *M* have produced similar results with further decreases in CPU time.

Table 2. CPU time ratios for the various methodologies for Cases 1 and 2.

Case	Average number of droplets in the steady state spray plume	Methodology (submodel)	CPU time / CPU time for complete simulation	CPU time / system time[§]
1*	26000	Discrete Charge	1	2.0×10^{7}
		Continuous Charge[¥]	0.0089	1.8×10^{5}
2**	3490	Discrete Charge	1	3.9×10^{5}
		Continuous Charge[¥]	0.113	4.4×10^{4}

*Park et al (2004)

**Tang and Gomez (1994)

[§]System time at the end of the simulation = 0.6 seconds.

[¥]*M* = 5000, *r** = 3 mm

4. Conclusions

Numerical simulations of electrospray droplets dynamics in the classical Lagrangian framework rely on the calculation of all droplet-to-droplet electrical interactions, which result in long computation times (CPU time). In contrast to this Discrete Charge approach, in this work we have explored the merits of a Continuous Charge submodel,

which approximates the spray to a continuous charge distribution, updated periodically as the plume evolves, from which the electrical field is solved using Gauss' law.

However, when applied to the entire spray this approach leads to unrealistic and highly distorted spray plume distributions. Instead, we have shown that this continuous approximation can be applied provided that different methods for computing the electrical force are used depending on the droplet's location. The electrical force on any droplets belonging to an 'outer' region RO, defined by a radius $r > r^*$, is computed from Gauss' law in terms of Poisson's equation whose source term is the continuous charge distribution representing the entire spray charge. On the other hand, the electrical force on any droplets belonging to an 'inner' region RI ($r \leq r^*$) has two contributions: the forces due to other droplets within region RI, which are accounted for one by one, and the forces due to droplets in RO, which are modeled as a continuous charge distribution.

This method takes advantage of the fact that the characteristic time scales for droplets' motion (microseconds) and for the global dynamics of the plume (milliseconds) are widely different. Since the global electrical field dynamics are much slower, the solutions of Poisson's equation are updated periodically, every several thousand time steps used in the integration of the droplets' motion equations.

We have applied this new methodology to simulate the spray dynamics for two real electrospray systems, described in the literature. The Discrete and the Continuous Charge submodels lead to minimal differences in the volumetric flux impinging on the collection plate, the droplet number density, and the droplet diameter distribution within the plume. For the system comprising 3490 droplets in the steady state, the use of the Continuous Charge submodel leads to a computational time which is only 11% of that

spent when the Discrete Charge submodel is used. For the system comprising 26000 droplets in the steady state, this computational time fraction is reduced to just 0.9%.

APPENDIX A. Confidence intervals for the flux distribution over the collecting plate

The flux distribution on the collecting plate along a radius, as presented in Figures 4 and 8, has been calculated according the following procedure.

First, we select a period Δt in the steady state portion of the simulation. The droplets impinging into the collection plate are sorted into bins representative of equal radially spaced rings $0, r_1, r_2 \ldots$, (where $\Delta r = r_m - r_{m-1}$ is constant). The impinging volumetric flux in bin m, is estimated as

$$f_m = \frac{\frac{1}{6}\sum_{l=1}^{N_m} d_l^3}{\left(r_m^2 - r_{m-1}^2\right)\Delta t} \tag{A.1}$$

where N_m is the number of droplets collected in bin *m* and d_l is the diameter of the l droplet. By this definition, f_m is a stochastic variable with some confidence interval, which should decrease as Δt increases.

This confidence interval can be estimated for a monodisperse electrospray (droplets with equal diameter *d*) considering the total number of droplets emitted in the period Δt, N_T, and the number of droplets collected in bin *m* over the same period, N_m. The probability that an emitted droplet is collected in bin *m* is p_m, which can be estimated as

$$\tilde{p}_m = \frac{N_m}{N_T} \tag{A.2}$$

Then, the number of total droplets collected follows a binomial distribution. The variance of the flux in bin *m* is then

$$Var(f_m) = \left[\frac{d^3}{6\left(r_m^2 - r_{m-1}^2\right)\Delta t}\right]^2 N_T p_m (1 - p_m) \tag{A.3}$$

If the spray is not monodisperse, the procedure is still applicable if we divide the span of diameters collected in bin *m* into *L* intervals. In this study we have taken equally spaced intervals, so

$$\Delta d_{m,k} = d_{m,k} - d_{m,k-1} = \left(d_{m,\max} - d_{m,\min}\right)/L; \;\; k = 1,...,L \tag{A.4}$$

A representative diameter for interval *k* is $\bar{d}_{m,k} = \left(d_{m,k} + d_{m,k-1}\right)/2$. Now the probability that a droplet with a representative diameter $\bar{d}_{m,k}$ is collected in bin *m,* is $p_{m,k}$, which can be estimated as

$$\tilde{p}_{m,k} = \frac{N_{m,k}}{N_{T,k}} \tag{A.5}$$

where $N_{T,k}$ is the total number of droplets with representative diameter $\bar{d}_{m,k}$ emitted in the period Δt, and $N_{m,k}$ is the number of droplets with representative diameter $\bar{d}_{m,k}$ collected in bin *m* in the same period. Because collecting droplets with different representative diameters are independent random events, the variance of the flux can be calculated as the sum of variances for the fluxes associated with each representative droplet diameter, as

$$Var(f_m) = \frac{1}{\left[6\left(r_m^2 - r_{m-1}^2\right)\Delta t\right]^2} \sum_{k=1}^{L} \bar{d}_{m,k}^6 N_{T,k} p_{m,k} \left(1 - p_{m,k}\right) \tag{A.6}$$

According to Box *et al.* (1978) a binomial distribution can be roughly estimated from the Normal distribution when $N_{T,k} > 5$ and $\left| \left[\sqrt{p_{m,k}/\left(1 - p_{m,k}\right)} - \sqrt{\left(1 - p_{m,k}\right)/p_{m,k}}\right] \Big/ \sqrt{N_{T,k}} \right| < 0.3$. The error bars in Figures 4 and 8 indicate one standard deviation (each side) which, under the Normal approximation,

represents a confidence interval of 68.3%. In these Figures, $\Delta r = 1.5\,\text{mm}$ and $L = 10$. When $L = 5$ the results differ by less than 1% from when $L = 10$.

Acknowledgements

This work was supported through projects DPI2012-35687 (Ministerio de Economía y Competitividad, Spain), and 2009SGR-01529 (Generalitat de Catalunya).

References

Abraham, F.F., Functional dependence of drag coefficient of a sphere on Reynolds number, Phys. Fluids 13(8) (1970) 2194-2195.

Arumugham-Achari, A.K., J. Grifoll, J. Rosell-Llompart, Two-way coupled numerical simulation of electrospray with induced gas flow, J. Aerosol Sci. 65 (2013) 121-133. doi: 10.1016/j.jaerosci.2013.07.005.

Bodnár, E., J. Rosell-Llompart, Growth dynamics of granular films produced by electrospray, J. Colloid Interf. Sci. 407 (2013) 536-545. doi: 10.1016/j.jcis.2013.06.013.

Box, G. E. P., Hunter, W. G. and Hunter, J. S., Statistics for Experimenters. Wiley (1978).

Barrero, A. and I. G. Loscertales, Micro- and nanoparticles via capillary flows, Annu. Rev. Fluid Mech. 39 (2007) 89-106. doi: 10.1146/annurev.fluid.39.050905.110245.

Bock, N., T. R. Dargaville, M. A. Woodruff. Electrospraying of polymers with therapeutic molecules: State of the art, Progr. Polym. Sci. 37(11) (2012) 1510-1551. doi: 10.1016/j.progpolymsci.2012.03.002.

Enayati, M., M.W. Chang, F. Bragman, M. Edirisinghe, E. Stride, Electrohydrodynamic preparation of particles, capsules and bubbles for biomedical engineering applications, Colloid Surface A. 382(1-3) (2011) 154-164. doi: 10.1016/j.colsurfa.2010.11.038

Fenn, J.B., Electrospray wings for molecular elephants (Nobel lecture), Angew. Chem. Int. Edit. 42 (33) (2003) 3871-3894. doi: 10.1002/anie.200300605.

Fernández de la Mora, J., The fluid dynamics of Taylor cones, Annu. Rev. Fluid Mech. 39 (2007) 217-243. doi: 10.1146/annurev.fluid.39.050905.110159.

Gañán-Calvo, A. M., J. C. Lasheras, J. Davila, A. Barrero, The electrostatic spray emitted from an electrified conical meniscus, J. Aerosol Sci. 25(6) (1994) 1121-1142.

Grifoll, J., J. Rosell-Llompart, Efficient Lagrangian simulation of electrospray droplets dynamics, J. Aerosol Sci. 47 (2012) 78-93. doi: 10.1016/j.jaerosci.2012.01.001.

Hartman, R.P.A., J.P. Borra, D.J. Brunner, J.C.M. Marijnissen, B. Scarlett, The evolution of electrohydrodynamic sprays produced in the cone-jet mode, a physical model, J. Electrostat. 47(3) (1999) 143-170. doi: 10.1016/S0304-3886(99)00034-0.

Higuera, F. J., Eulerian model of a dilute spray of charged droplets, J. Aerosol Sci. 48 (2012) 34-45. doi: 10.1016/j.jaerosci.2012.01.008.

Higuera, F.J., Multifluid Eulerian model of an electrospray in a host gas, J. Fluid Mech. 734 (2013) 363-386. doi: 10.1017/jfm.2013.450.

Jaworek, A., A.T. Sobczyk, Electrospraying route to nanotechnology: An overview, J. Electrostat. 66 (3-4) (2008) 197-219. doi: 10.1016/j.elstat.2007.10.001.

Jaworek, A., Electrospray droplet sources for thin film deposition, J.Mater. Sci. 42 (2007a) 266-297. doi: 10.1007/s10853-006-0842-9.

Jaworek, A., Micro- and nanoparticle production by electrospraying, Powder Technol. 176(1) (2007b) 18-35. doi: 10.1016/j.powtec.2007.01.035.

Martin, S., P.L. Garcia-Ybarra, J.L. Castillo, Electrospray deposition of catalyst layers with ultra-low Pt loadings for PEM fuel cells cathodes, J. Power Sources 195(9) (2010) 2443-2449. doi: 10.1016/j.jpowsour.2009.11.092.

Park, H., K. Kim, S. Kim, Effects of a guard plate on the characteristics of an electrospray in the cone-jet mode, J. Aerosol Sci. 35(11) (2004) 1295-1312. doi: 10.1016/j.jaerosci.2004.05.012.

Peltonen, L., H. Valo, R. Kolakovic, T. Laaksonen, J. Hirvonen, Electrospraying, spray drying and related techniques for production and formulation of drug nanoparticles, Expert Opin. Drug Del. 7(6) (2010) 705-719. doi: 10.1517/17425241003716802.

Rietveld, I.B., K. Kobayashi, H. Yamada, K. Matsushige, Electrospray deposition producing ultra-thin polymer films with a regular surface structure, Soft Matter 5(3) (2009) 593-598. doi: 10.1039/b812702f.

Tang, K., A. Gomez, On the structure of an electrostatic spray of monodisperse droplets, Phys. Fluids 6(7) (1994) 2317-2332.

Wilhelm, O., L. Madler, S.E. Pratsinis, Electrospray evaporation and deposition, J. Aerosol Sci. 34(7) (2003) 815-836. doi: 10.1016/S0021-8502(03)00034-X.

Zamani, M., M. P. Prabhakaran, S. Ramakrishna, Advances in drug delivery via electrospun and electrosprayed nanomaterials, Int. J. Nanomed. 8 (2013) 2997-3017. doi: 10.2147/IJN.S43575.

Yang, W., B. Lojewski, Y. Wei, W, Deng, Interactions and deposition patterns of multiplexed electrosprays, J. Aerosol Sci. 46 (2012) 20-33 doi: 10.1016/j.jaerosci.2011.11.004.

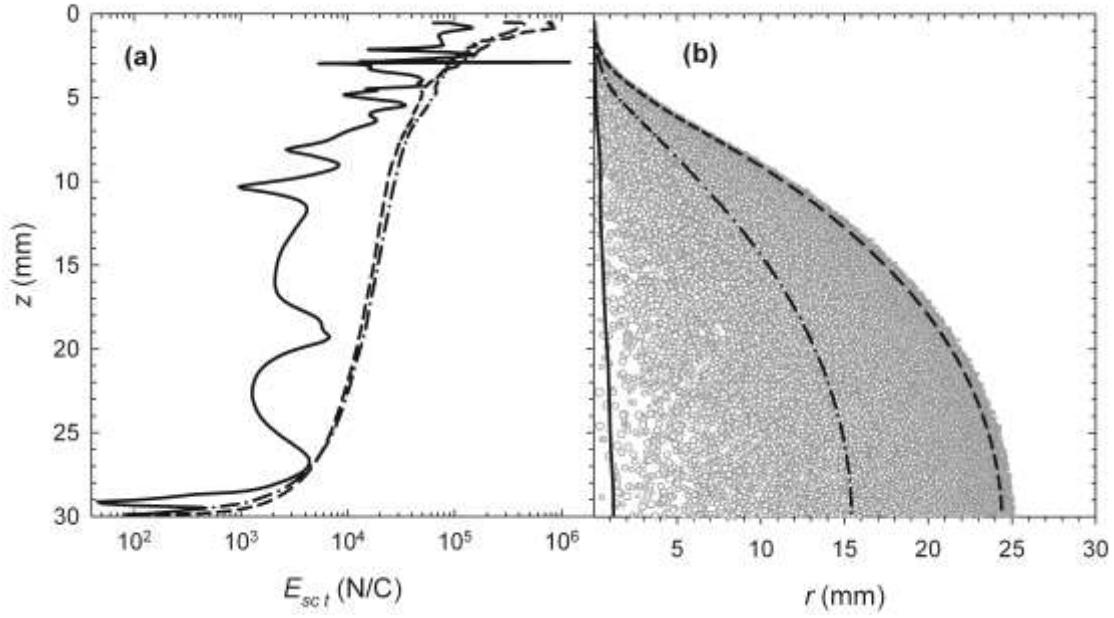

Figure 1. (a) Modulus of the transversal component of the space charge field experienced by three droplets as they travel through an example spray. (b) Projection in the in *rz*-plane of the trajectories of the same droplets, overlaid on a snapshot of droplets' positions, wherein each symbol diameter is proportional to the droplet diameter. (This spray coincides with Case 1 in this study.)

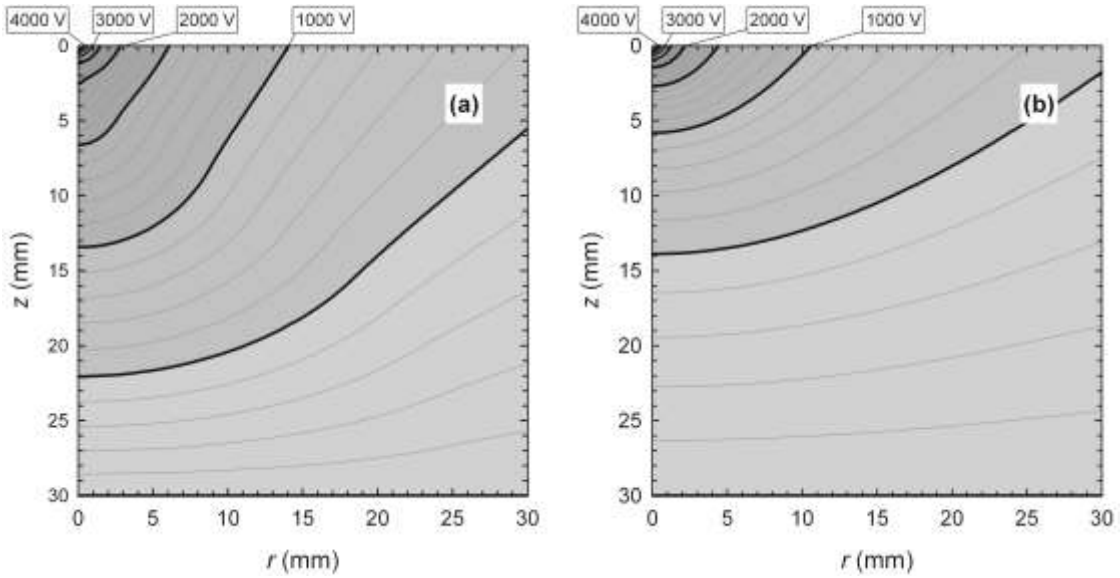

Figure 2. Contour plots of the electrical potential for Case 1: (a) considering the electrodes and the charge density field from a single snapshot; (b) considering only the electrodes.

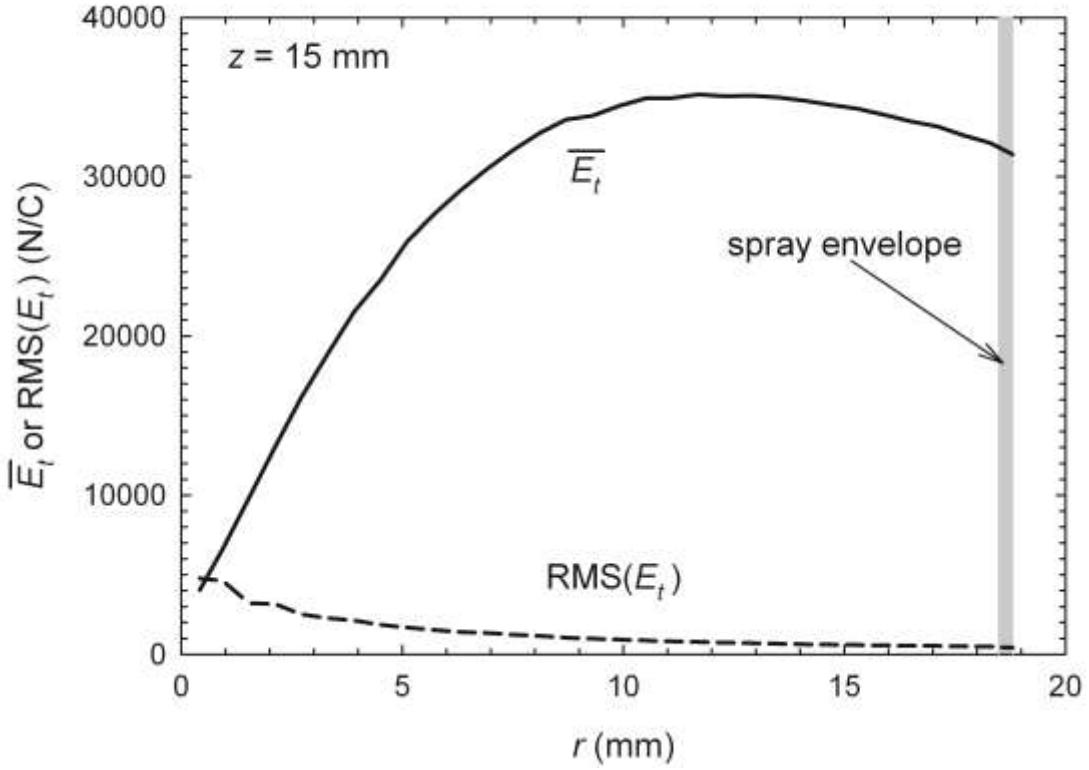

Figure 3. Average and RMS of the transversal component of the electrical field *versus r* for Case 1. This figure is built from droplets in a slice defined by $14.5 < z < 15.5$ mm, for 2500 snapshots of the spray taken at regular intervals within the period 0.1 to 0.6 seconds.

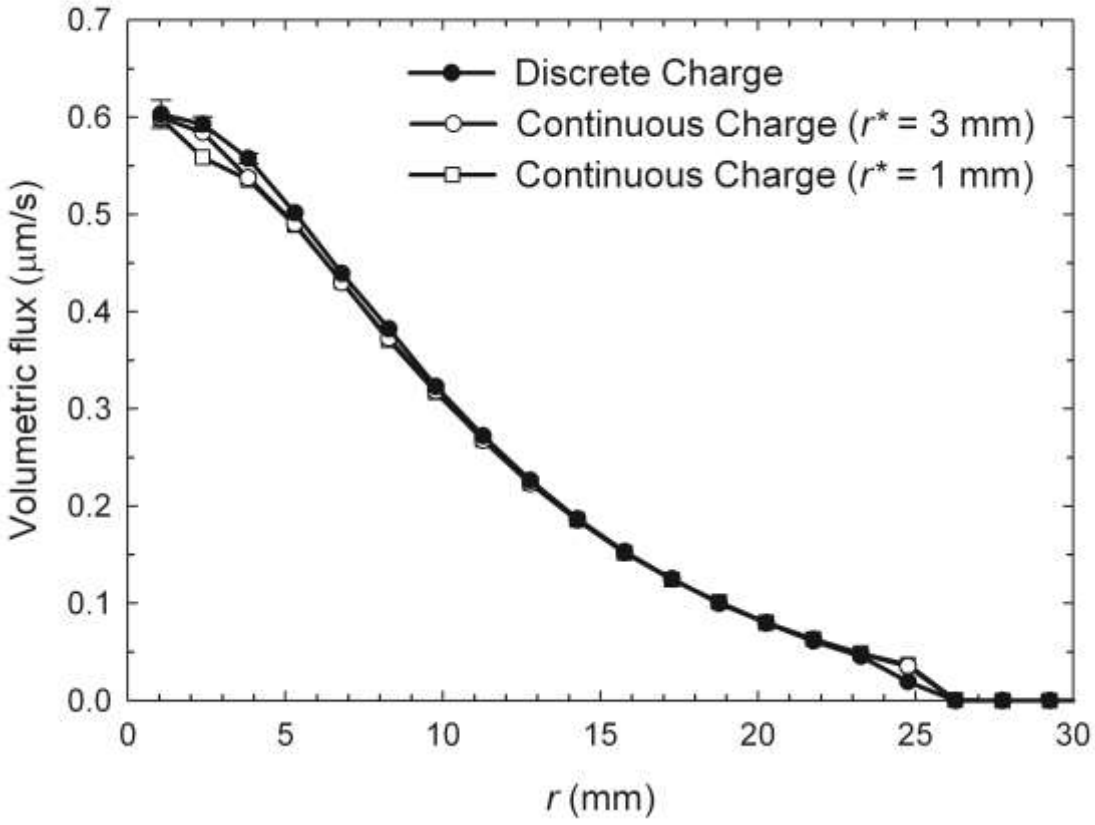

Figure 4. Radial distribution of the volumetric flux impinging on the collection plate for Case 1, obtained using the Discrete Charge submodel and the Continuous Charge submodel with M = 5000 and two values of r^*. Uncertainty bars represent 68.3% confidence intervals. This figure is built from 2500 snapshots taken at regular intervals within the period 0.1 to 0.6 seconds.

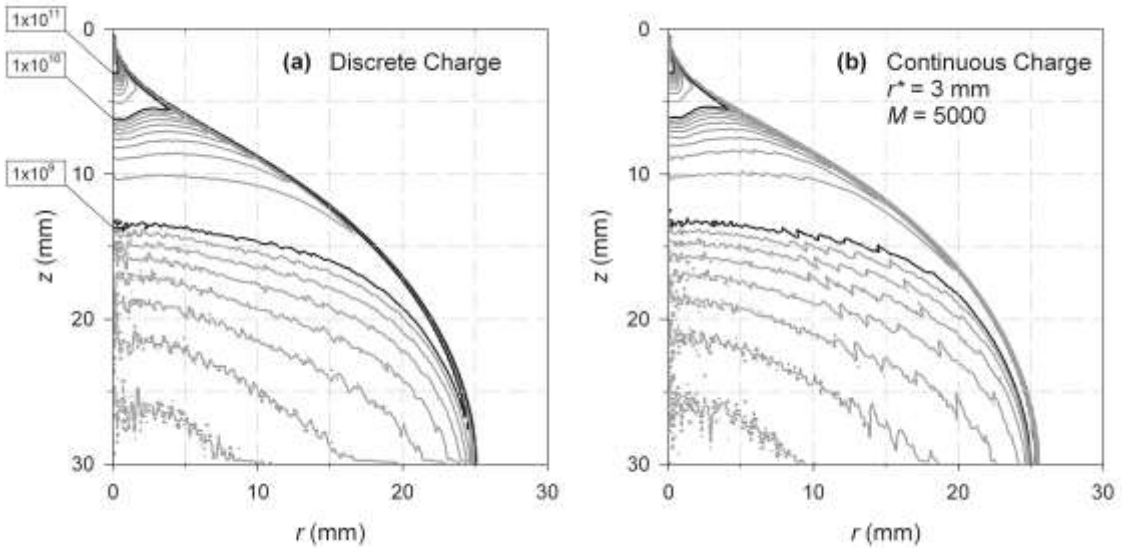

Figure 5. Average droplet number density (#/m^3) contour plots for Case 1, obtained with (a) Discrete Charge submodel, and (b) Continuous Charge submodel. This figure is built from 2500 snapshots taken at regular intervals within the period 0.1 to 0.6 seconds.

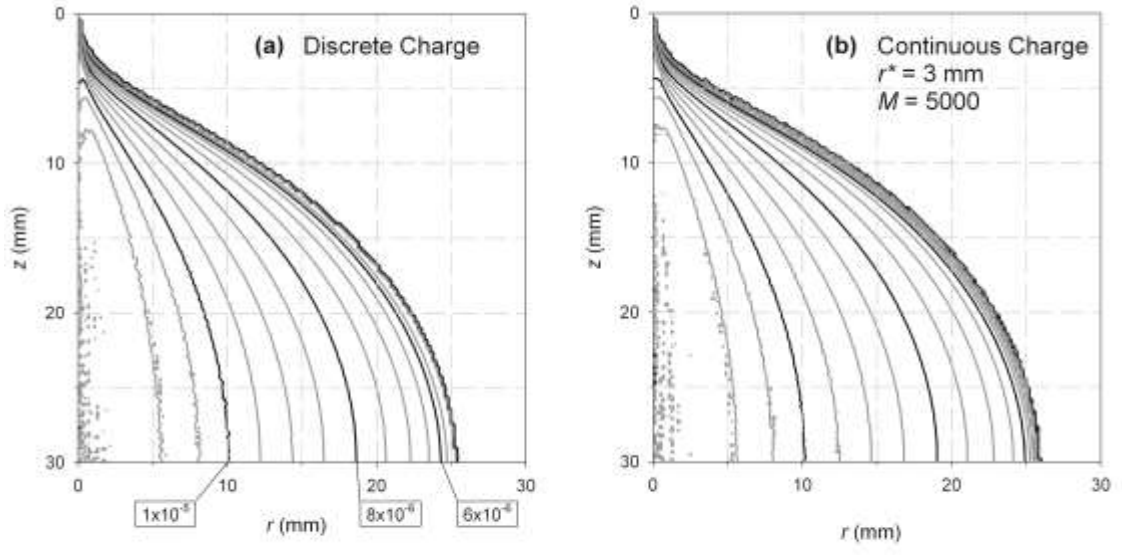

Figure 6. Average droplet diameter (m) contour plots for Case 1, obtained with (a) Discrete Charge submodel, and (b) Continuous Charge submodel. This figure is built from 2500 snapshots taken at regular intervals within the period 0.1 to 0.6 seconds.

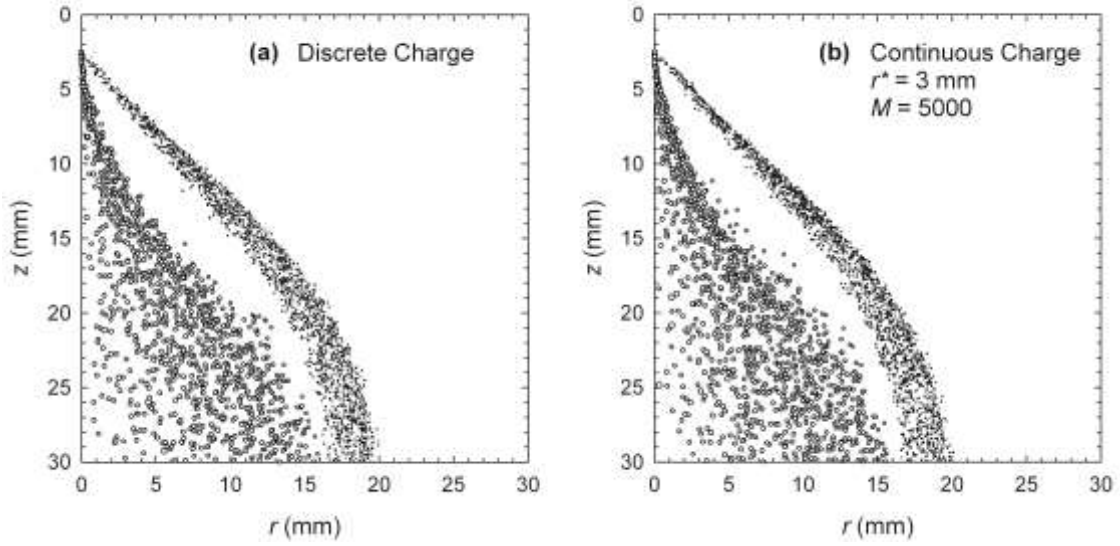

Figure 7. Snapshots of droplets' positions in *rz*-plane for Case 2 (at time 0.6 seconds), obtained with (a) Discrete Charge submodel, and (b) Continuous Charge submodel. Each symbol diameter is proportional to the droplet diameter.

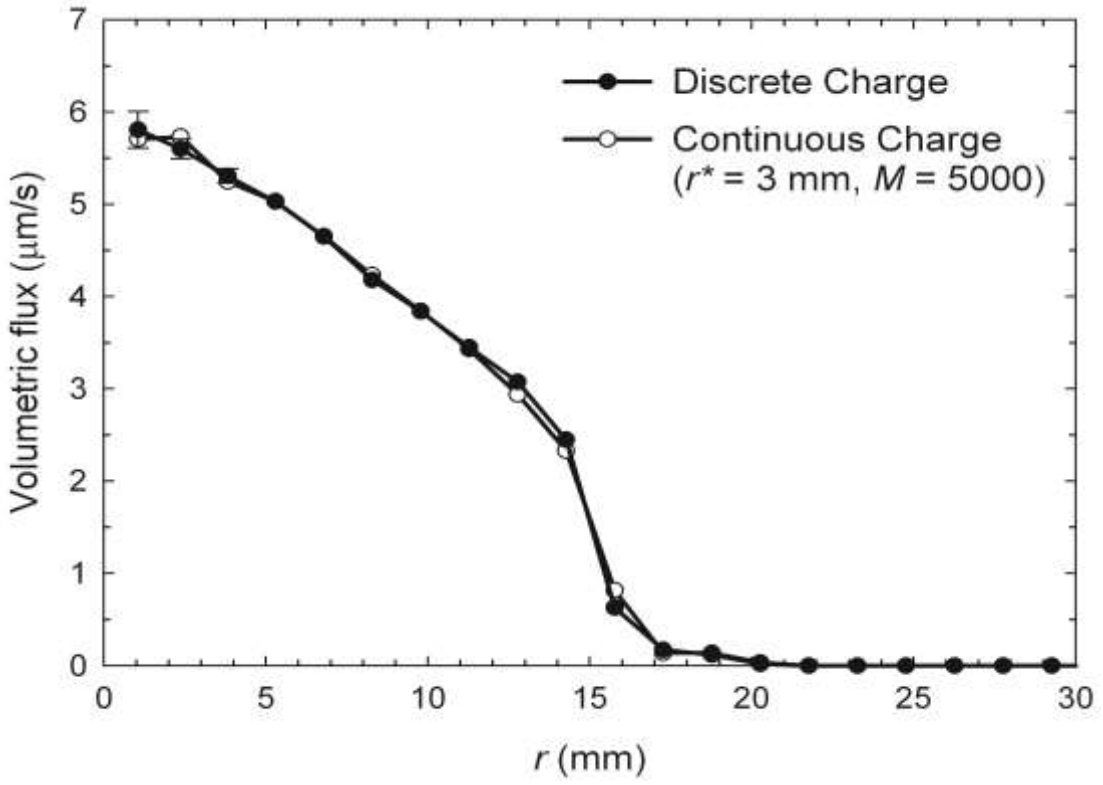

Figure 8. Radial distribution of the volumetric flux impinging on the collection plate for Case 2, obtained using the Discrete Charge submodel and the Continuous Charge submodel. Uncertainty bars represent 68.3% confidence intervals. This figure is built from 2500 snapshots taken at regular intervals within the period 0.1 to 0.6 seconds.